

Imperfection effects for multiple applications of the quantum wavelet transform

M. Terraneo and D. L. Shepelyansky*

*Laboratoire de Physique Quantique, UMR 5626 du CNRS,
Univ. Paul Sabatier, 31062 Toulouse Cedex 4, France*

(Dated: March 9, 2003)

We study analytically and numerically the effects of various imperfections in a quantum computation of a simple dynamical model based on the Quantum Wavelet Transform (QWT). The results for fidelity timescales, obtained for a large range of error amplitudes and number of qubits, imply that for static imperfections the threshold for fault-tolerant quantum computation is decreased by a few orders of magnitude compared to the case of random errors.

PACS numbers: 03.67.Lx, 43.60.Hj, 05.45.M

The mathematical theory of Wavelet Transforms (WT) finds nowadays an enormous success in various fields of science and technology, including treatment of large databases, data and image compression, signal processing, telecommunications and many other applications [1, 2]. Wavelets are obtained by translations and dilations of an original function and they allow to obtain high resolutions of microscopic details, both in frequency and space. The discrete WT can be implemented with high computational efficiency and provide a powerful tool for treatment of digital data. It is well accepted that the Fourier transform and WT are the main instruments for data treatment, and it has been shown that in many applications the performance of WT is much higher compared to the Fourier analysis. The permanent growth of computer capacity has significantly increased the importance of the above transformations in numerical applications.

The recent development of quantum information processing has shown that computers based on laws of quantum mechanics can perform certain tasks exponentially faster than any known classical computational algorithms (see *e.g.* [3]). The most known example is the integer factorization algorithm proposed by Shor [4]. An essential element of this algorithm is the Quantum Fourier Transform (QFT) which can be performed for a vector of size $N = 2^{n_q}$ in $O(n_q^2)$ quantum gates, in contrast to $O(2^{n_q} n_q)$ classical operations [3, 4]. Here n_q can be viewed as the number of qubits (two-level quantum systems) of which a quantum computer is built. Apart from Shor's algorithm, the QFT finds a number of various applications in quantum computation, including the simulation of quantum chaos models showing rich and complex dynamics [5, 6, 7]. The sensitivity of the QFT to imperfections was tested in numerical simulations and the time-scales for reliable computation of the algorithm were established [6, 7, 8, 9].

A few years after the discovery of the QFT algorithm, it has been shown that certain WT can also be implemented on a quantum computer in a polynomial number of quantum gates [10, 11, 12]. In fact, explicit quantum circuits were developed for the most popular discrete

WT, namely the 4-coefficient Daubechies WT ($D^{(4)}$) and the Haar WT, both for pyramidal and packet algorithms [10, 11, 12]. As it happens in classical signal analysis, it is natural to expect that QWT will find important future applications for the treatment of quantum databases and quantum data compression. Therefore, it is important to investigate the stability and the accuracy of QWT in respect to imperfections. This is especially important since the functions of the wavelet basis have singularities in the derivatives (in contrast to analyticity of Fourier waves) that may enhance the effects of perturbations.

To this aim we introduce a simple model with rich nontrivial dynamics which is essentially based on multiple applications of the WT. Its quantum evolution can be efficiently simulated on a quantum computer, and it is described by the unitary map for the wave function ψ :

$$\bar{\psi} = \hat{U}\psi = \hat{W}^\dagger e^{-ik(x-\pi)^2/2} \hat{W} e^{-iTn^2/2} \psi. \quad (1)$$

Here the bar marks the value of the wave function after one map iteration, \hat{W} is the $D^{(4)}$ WT operator, and the unitary diagonal operators $U_T = e^{-iTn^2/2}$ and $U_k = e^{-ik(x-\pi)^2/2}$ represent quantum phase rotation in computational and wavelet basis, respectively. The evolution takes place in the Hilbert space of $N = 2^{n_q}$ states, with $-N/2 \leq n < N/2$ and $x = 2\pi j/N$ where $j = 0, \dots, N-1$ is the index in the wavelet basis and T, k are dimensionless parameters. In the case when \hat{W} is replaced by the Fourier transform, one obtains the quantum sawtooth map previously analyzed in Ref.[7]. Thus the model (1) can be considered as a 'kicked wavelet rotor', where k is the kick strength in the wavelet basis. We numerically tested that the dynamical properties are not very sensitive to the value of T and here we present data for a typical value $T = 1.4$.

The global properties of the evolution operator (1) are shown in Figs.1,2 for different values of k (see also Appendix A1). The density plot of transition matrix elements $U_{n,n'}$ in the computational basis is represented in Fig.1. By increasing k a larger and larger number of states is coupled by the dynamics, and the complex self-similar structure of the transitions generated by the WT

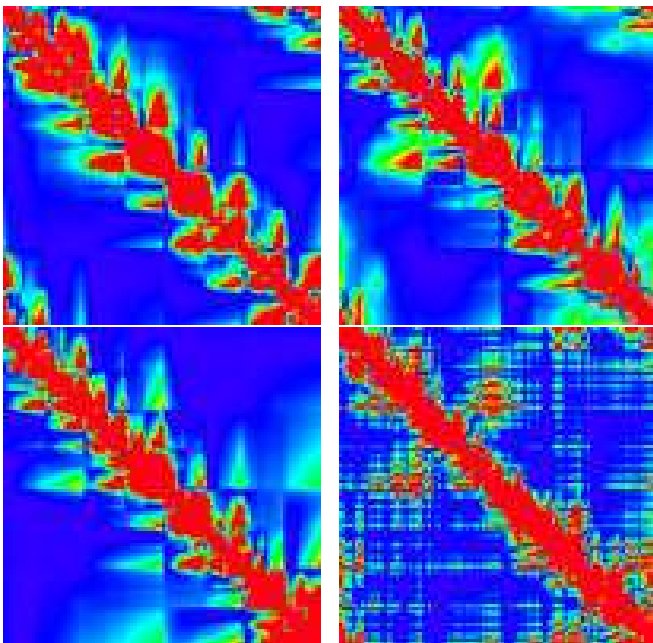


FIG. 1: (Color on line) Density plot of matrix elements $|U_{n,n'}|^2$ for the model (1) in the computational basis, for $N = 2^{12}$. Top: $k = 100$ (left), $k = 1000$ (right); bottom is for $k = 1000$: a doubled resolution of left upper quarter (left), perturbed operator with static errors $\epsilon = 5 \times 10^{-4}$, $\mu = 0$. Color marks the density from blue (zero) to red (maximal value).

becomes evident. On the average, the off-diagonal matrix elements decay with the power law $|U_{n,n'}|^2 \sim 1/|n-n'|^\alpha$. Asymptotically for $|n-n'| \gg 5k$ we obtain the exponent $\alpha = 4$ (Fig.2). For large values of k the intermediate scaling law is described by the exponent $\alpha = 2$, in the range $1 \leq |n-n'| \ll 5k$. This decay law for the matrix elements can be considered as a long range coupling between states. We note that similar power law regimes have been analyzed in random matrix models [13, 14]. Our numerical analysis shows that there are two regimes for the level spacing statistics $P(s)$ [15] in the limit of large N . *E.g.* for $N = 2^{12}$ the distribution $P(s)$ is given by the Poisson law for $k < 5$, while for $5 < k \leq 10000$ it shows level repulsion and a poissonian decay for large s (see Appendix A2). We attribute the rapid appearance of level repulsion to the slow power law decay of matrix elements [14].

To implement the evolution (1) on a quantum computer, we developed an algorithm based on the QWT for the Daubeschies $D^{(4)}$ wavelets. The algorithm consists of four steps: i) the multiplication by \hat{U}_T , performed in $O(n_q^2)$ controlled-phase shift gates as described in [7]; ii) the application of \hat{W} operator, realized by the QWT following the circuit described in Fig.10 of [11] (see Appendix A3); iii) the operator \hat{U}_k , implemented in a similar way as for the step i); iv) the inverse WT \hat{W}^\dagger , obtained by reversing the gates of the step ii). The heaviest parts

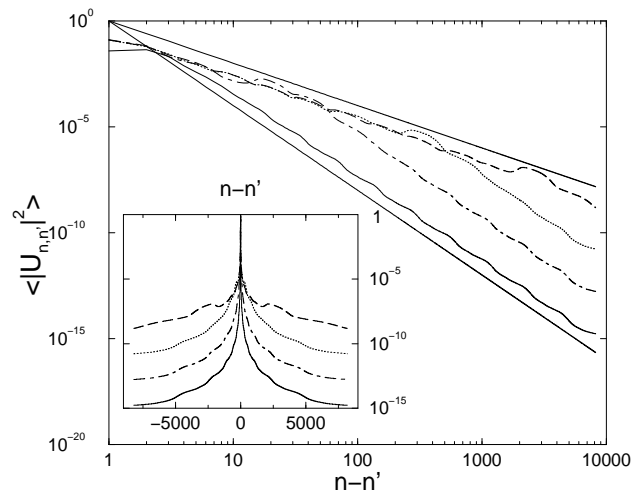


FIG. 2: Dependence of averaged matrix elements $\langle |U_{n,n'}|^2 \rangle$ on $|n-n'|$ (the average is taken along the diagonal). Data are shown for $N = 2^{15}$ and $k = 1$ (full black curve), $k = 10$ (dash-dotted curve), $k = 100$ (dotted curve) and $k = 1000$ (dashed curve). The two straight lines are $1/|n-n'|^2$ and $1/|n-n'|^4$. The inset shows the data in semi-log scale.

of the algorithm are the steps ii), iv), since the QWT algorithm requires multi-controlled operations. To implement them we used the recipe given in [16] which allows to realize a n -controlled gate by $O(n)$ elementary gates (Toffoli and 1- and 2-qubit gates). To this end an ancilla qubit is needed, so that we used $n_q + 1$ qubits to simulate numerically the dynamics of model (1) with $N = 2^{n_q}$ states. The implementation of the wavelet kernel $D_{2^n}^{(4)}$ requires $O(n)$ multi-controlled gates ($n = 2, \dots, n_q$), and since the QWT is composed of $O(n_q)$ kernel applications this leads the total number of elementary gates to scale as $O(n_q^3)$ [10, 11, 12] (see Appendix A3). To study the algorithm accuracy we consider two models of imperfections. In the model of random noisy gates we replace all ideal gates by imperfect ones, which are obtained by random unitary rotations by a small angle η , $-\epsilon/2 \leq \eta \leq \epsilon/2$, around the ideal rotation angle (as in [17]). In the model of static imperfections (see [7, 18]) all gates are perfect but between gates ψ accumulates a phase factor $e^{i\phi}$ with $\phi = \sum_l (\eta_l \sigma_l^z + \mu_l \sigma_l^x \sigma_{l+1}^x)$. Here η_l, μ_l vary randomly with $l = 0, \dots, n_q$, η_l represents static one-qubit energy shifts, $-\epsilon/2 \leq \eta_l \leq \epsilon/2$, and μ_l represents static inter-qubit couplings on a circular chain, $-\mu/2 \leq \mu_l \leq \mu/2$.

The numerical simulations of the ideal quantum algorithm for the map (1) show that the wave function is essentially localized on a few states of the computational basis. This localization is clearly seen from the Inverse Participation Ratio (IPR) $\xi = 1/\sum_n |\psi_n|^4$ which is a standard quantity to characterize localization in mesoscopic systems [15]. It directly provides the number of sites on which the probability is concentrated. Surprisingly the localization is present not only for moderate $k \sim 1$, but also when the kick strength is very large

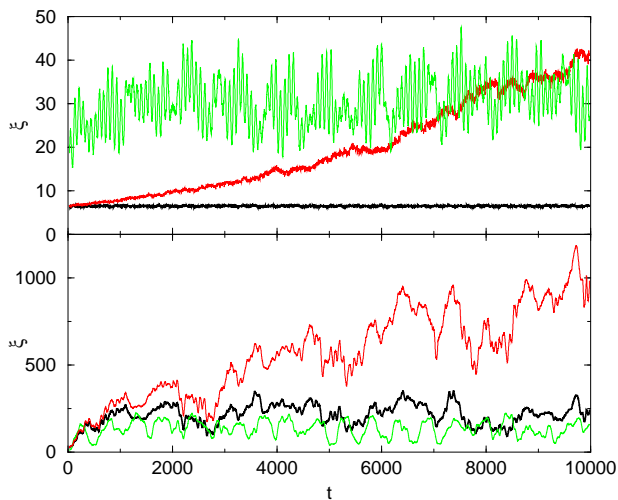


FIG. 3: (Color on line) Dependence of IPR ξ on the number of iterations t , for $n_q = 12$, $T = 1.4$, $k = 1$ (top) and $k = 1000$ (bottom). Initially the probability is concentrated at $n = 0$. The black curves show the quantum computation with ideal gates; the green (light gray) curves show the case with static errors at $\epsilon = 10^{-4}$, $\mu = 0$ and red (gray) curves correspond to the case with noisy gates at $\epsilon = 5 \times 10^{-4}$. The data are averaged over time interval $\Delta t = 50$.

$k \sim 1000$ (see Fig. 3 and Appendix A4). Indeed in both cases ξ fluctuates near a constant value $\xi_0 \ll N$, even for a very large number of iterations. We attribute this localization to the structure of the operator (1): it is banded for moderate k and sparse for large k (see Fig.(1)). For $k \sim 1$ the probability shows an algebraic localization $|\psi_n|^2 \propto 1/n^4$ (Fig.4). Such an exponent fully agrees with the scaling law of Fig.2. For $k > 100$, the probability is spread over the whole basis (data not shown), but only a moderate number of narrow peaks contributes to the IPR value (see Fig.3). This behaviour is consistent with the fact that the $P(s)$ never reaches a Wigner-Dyson regime (see discussion above). On the contrary, the spectral properties of the sawtooth map [7, 19] are described by the random matrix theory for $k \sim 1000$, $T \sim 1$ and $N = 2^{12}$.

The effect of imperfections in the quantum gates is shown in Figs. 3, 4 (see also Appendix A4). The results clearly show that the localization is destroyed by noisy gates imperfections which lead to an approximately linear growth of ξ with t . For static imperfections ξ shows modified bounded oscillations. The probability distribution in Fig.4 shows the appearance of a plateau with pronounced peaks located approximately at $n = N/2^m$, $m = 1, 2, 3, \dots$. We attribute the appearance of these peaks to the pyramidal structure of the algorithm, which in the presence of imperfections produces stronger errors at the above values of n . For static imperfections the plateau level remains bounded in time t while for noisy gates it increases with t and for very large t the probability becomes homogeneously distributed over the

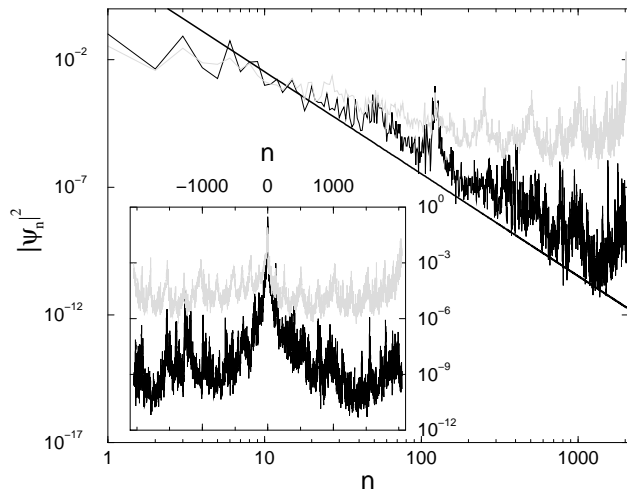


FIG. 4: Probability distribution $|\psi_n|^2$ in the computational basis for the parameters of Fig.3 (top) at $k = 1$, $t = 10^4$: full curve is the quantum computation with ideal gates, gray curve shows data for noisy gates with $\epsilon = 5 \times 10^{-4}$. The straight line displays the scaling law $1/n^4$. The inset shows the same data in semilogarithmic scale.

computational basis.

The qualitative difference between two types of imperfections becomes clear from the analysis of the behaviour of the fidelity, defined as $f(t) = |\langle \psi_\epsilon(t) | \psi(t) \rangle|^2$. Here $\psi(t)$ is the wave function obtained with ideal gates, while $\psi_\epsilon(t)$ is the result of the quantum computation with imperfections of amplitude ϵ . We determine the time scale t_f for accurate computation by fixing a threshold for the fidelity as $f(t_f) = 0.9$. In this way it is possible to find the dependence of t_f on the system parameters. Our numerical data are presented in Fig.5. They show that for noisy gates t_f is described by the relation

$$t_f = C/(\epsilon^2 n_g), \quad N_g = C/\epsilon^2 \quad (2)$$

where n_g is the number of gates per map iteration, $N_g = n_g t_f$ is the total number of gates and $C \approx 5$ is a numerical constant. The physical origin for this scaling is related to the fact that after each gate an amount of probability of the order of ϵ^2 is transferred from the ideal state to all other states. This leads to an exponential decay of the fidelity $f(t) \approx \exp(-A\epsilon^2 n_g t)$, where A is a constant (see Fig.5a). This gives the scaling (2), which was also found in other algorithms with noisy gates [7, 9, 17].

For the model with static imperfections the scaling is

$$t_f = D/(\epsilon n_g n_q^{1/2}), \quad N_g = D/(\epsilon n_q^{1/2}) \quad (3)$$

where D is a numerical constant ($D \approx 4.5$, at $\mu = 0$ and $D \approx 2.1$ at $\mu = \epsilon$). This timescale is significantly smaller than the one for noisy gates. Physically, this happens due to the coherent action of static imperfections, which lead to effective Rabi oscillations proportional to $\cos(\epsilon n_g t)$ for each qubit. For n_q qubits this gives $f(t) \propto [\cos(\epsilon n_g t)]^{n_q}$

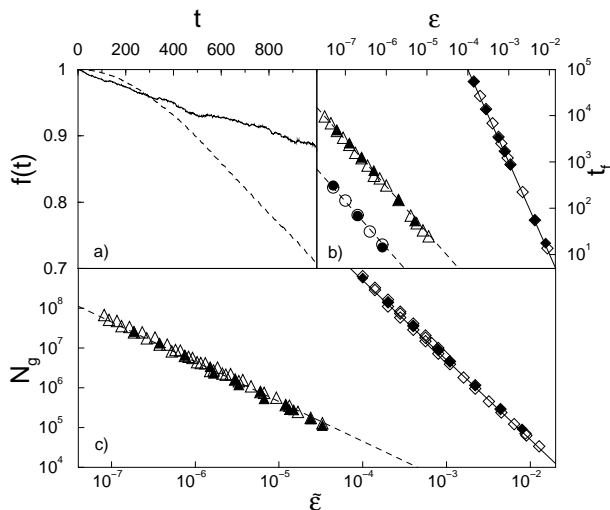


FIG. 5: Panel a) shows the fidelity decay in time at $k = 1$, $n_q = 12$ for static imperfections ($\epsilon = 10^{-4}$, $\mu = 0$, dashed curve) and noisy gates ($\epsilon = 5 \times 10^{-4}$, full curve). Panel b) shows the dependence of time scale t_f on the imperfection strength ϵ for $n_q = 8$ ($n_g = 5237$) for noisy gates (diamonds) and static imperfections (triangles at $\mu = 0$; circles at $\mu = \epsilon$, for clarity data are shifted in ϵ -axis by factor 10 to the left). Panel c) gives the dependence of the total number of gates N_g on $\tilde{\epsilon}$ for $n_q = 6, 8, 10$. For noisy gates (diamonds) $\tilde{\epsilon} = \epsilon$ and for static imperfections (triangles) $\tilde{\epsilon} = \epsilon\sqrt{n_q}$. Open (full) symbols are data for $k = 1$ ($k = 1000$). The full and dashed lines in panels b)/c) show the relations (2) and (3), respectively.

and for small ϵ we obtain a Gaussian drop of the fidelity $f(t) \sim \exp(-n_q(\epsilon n_g t)^2)$, in agreement with our numerical results (see Fig.5a). This leads to the scaling (3), which is confirmed by the data in Fig.5. The effects of static imperfections are dominant for all range of imperfection strengths studied. We note that the scaling laws (2), (3) are rather general and do not depend on the kick strength k . We note that similar scalings were discussed and numerically demonstrated in other quantum algorithms with noisy gates [9, 17] and static imperfections [7] (see also [20]). This shows that such scaling laws are generic and are not sensitive to the singularities in the derivatives of the wavelets. The universality of the above relations (2), (3) is also confirmed by the fact that the

structure of the QWT is rather different from the QFT algorithm, *e.g.* the number of elementary quantum gates scales as $O(n_q^3)$ for the QWT, in contrast to $O(n_q^2)$ for the QFT. These relations determine the total number of gates $N_g = t_f n_g$ during which the quantum computation is reliable. Similar scalings for N_g should also be valid for other quantum algorithms, *e.g.* Grover's and Shor's algorithms. We discuss also other types of errors in Appendix A5.

The above relations (2), (3) are important for the quantum error correction codes and the fault-tolerant quantum computation threshold (see [3, 21] and Refs. therein). Indeed the accuracy border for large scale quantum computation is obtained in the assumptions of random noisy errors and gives a threshold $\epsilon < \epsilon_r \sim 10^{-2}$. This approach intrinsically uses the fact that for noisy gates the fidelity remains close to one for a number of gates $N_g = C/\epsilon_r^2$ (see (2)). In the case of static imperfections it is natural to assume that this number of gates should remain approximately the same to allow large scale computation on a quantum computer with n_q qubits. Therefore, for static imperfections the Eqs. (2), (3) give the accuracy border ϵ_s :

$$\epsilon_s \approx D\epsilon_r^2 / (Cn_q^{1/2}) \quad (4)$$

This important relation gives a significant decrease of the threshold for the case of static imperfections [22]. For the parameters of our model at $n_q = 10$ we obtain that for the noisy error rate $p_r = \epsilon_r^2 \approx 10^{-4}$ the rate induced by static imperfections should be less than $p_s = \epsilon_s^2 \approx 10^{-9}$. This result shows that new strategies of quantum error correction codes should be developed to significantly suppress phase shifts induced by static imperfections. The spin echo techniques used in NMR [3] may play here an important role.

This work was supported in part by the EC contracts RTN QTRANS and IST-FET EDIQIP and the NSA and ARDA under ARO contract No. DAAD19-01-1-0553. We thank CalMiP in Toulouse and IDRIS at Orsay for access to their supercomputers.

APPENDIX

A1

Here we show examples of density plot for the matrix elements $|U_{n,n'}|^2$ for the model (1) for $k = 1, 10, 100, 1000$ (Fig.6).

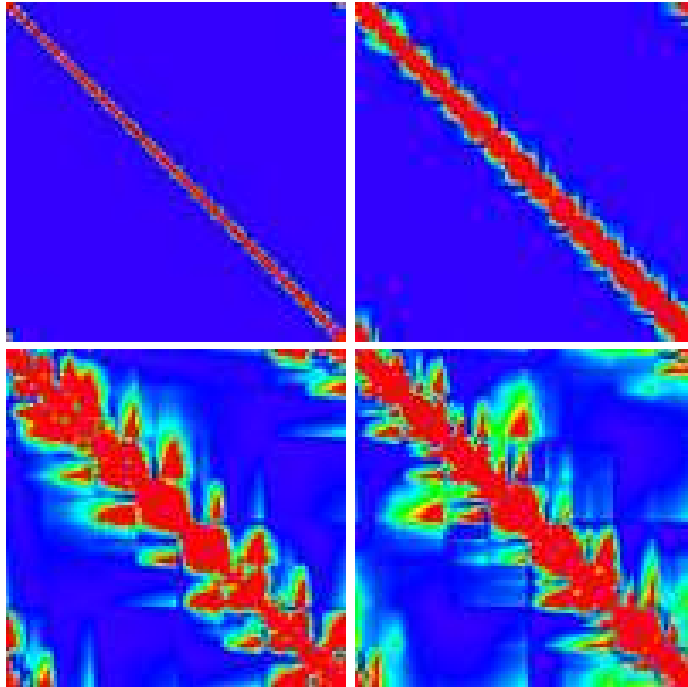


FIG. 6: Density plot of matrix elements $|U_{n,n'}|^2$ for the model (1) in the computational basis, for $N = 2^{12}$, $k = 1$ (top left), $k = 10$ (top right), $k = 100$ (bottom left) and $k = 1000$ (bottom right). Color marks the probability density, from blue to red (maximal value).

A2

The spectral analysis of the model (1) is obtained by a numerical diagonalization of the evolution operator \hat{U} . Due to the unitarity of \hat{U} , all the eigenvalues λ are on the unitary circle, $\lambda = e^{i\omega}$, where ω are the quasi-energies included in the interval $[0, 2\pi)$. The typical examples for the level spacing statistics $P(s)$ for ω are shown in Fig.7. It is remarkable that even for large kick strengths (*e.g.* $k = 1000$) the Wigner-Dyson statistics of the random matrix theory is not achieved. We note that for such values of k in the sawtooth map all the eigenstates are delocalized and $P(s)$ is given by the Wigner-Dyson distribution [7, 19].

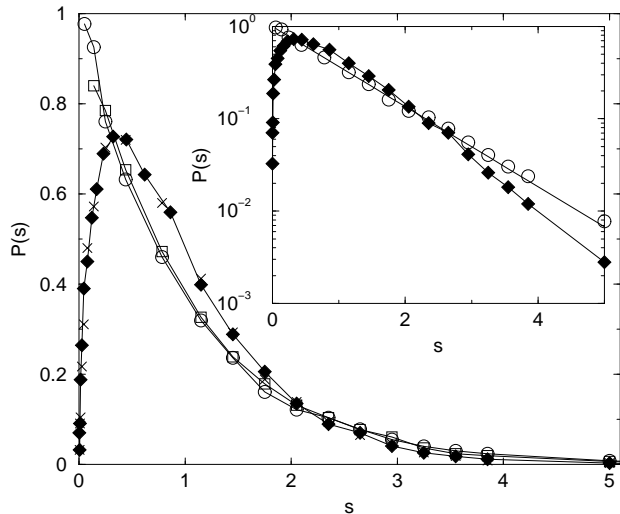


FIG. 7: Level spacing statistics $P(s)$ for the quasi-energies of model (1), for $n_q = 12$ and different values of the parameter k . A transition from the Poisson distribution $P(s) = e^{-s}$ at small k values to a distribution which shows the level repulsion for small s is observed by increasing k . Data are shown for $k = 0.1$ (squares), $k = 1$ (circles), $k = 10$ (diamonds) and $k = 1000$ (\times 's). The inset displays the data for $k = 1$ and $k = 10$ in a semilogarithmic scale. The full line is the Poisson distribution.

A3

Our quantum circuit is based on the scheme described in [11]. We implemented the Pyramidal Algorithm (PYA) for the $D^{(4)}$ wavelet transform. It is based on repeated applications of the operator $D_{2^n}^{(4)}$ (the wavelet kernel) and the permutation operator Π_{2^n} . Here the kernel $D_{2^n}^{(4)}$ is the Daubechies $D^{(4)}$ matrix of size $2^n \times 2^n$. The operator Π_{2^n} realizes the shuffling step on vectors $\{v_j\}_{j=1,2^n}$ of size 2^n . The action of Π_{2^n} can be regarded as a (classical) permutation of the index for the vector $\{v_j\}_{j=1,2^n}$. The binary representation of index j , $(a_0, a_1, \dots, a_{n-1})$, is mapped into $(a_{n-1}, a_0, a_1, \dots, a_{n-2})$, where a_0 is the most significant bit. The classical operator $D^{(4)}$ can be written as

$$D^{(4)} = (D_4^{(4)} \oplus I_{2^{n_q-4}})(\Pi_8 \oplus I_{2^{n_q-8}}) \dots (D_{2^i}^{(4)} \oplus I_{2^{n_q-2^i}})(\Pi_{2^{i+1}} \oplus I_{2^{n_q-2^{i+1}}}) \dots \Pi_{2^{n_q}} D_{2^{n_q}}^{(4)} \quad (5)$$

where I_M is the identity matrix of size $M \times M$ and \oplus is the direct sum of operators (see Fig.8).

In a quantum computation, the action of Π_{2^n} on the element $|j\rangle = |a_0, a_1, \dots, a_{n-1}\rangle$ of the computational basis is $\Pi_{2^n}|a_0, a_1, \dots, a_{n-2}, a_{n-1}\rangle = |a_{n-1}, a_{n-2}, \dots, a_1, a_0\rangle$ and it can be implemented via $n-1$ quantum swaps, each of them built by 3 control-not gates. The direct sums $\Pi_{2^n} \oplus I_{2^{n_q-2^n}}$ and $D_{2^n}^{(4)} \oplus I_{2^{n_q-2^n}}$ correspond to multi-controlled operators with $n_q - n$ controlling qubits. Both Π_{2^n} and $D_{2^n}^{(4)}$ can be implemented by a polynomial sequence of elementary gates (Toffoli, Control-Not, and one-qubit rotations), therefore the above multi-controlled operators are replaced by the product of multi-controlled elementary gates. Following the procedure proposed in [16], these multi-controlled gates were implemented through elementary gates with the help of an ancilla qubit. The computational cost of a l -controlled gate is linear in the number of controlling qubits l .

The wavelet kernel $D_{2^n}^{(4)}$ is decomposed into elementary gates following the factorization proposed in [11] with slight modifications. The kernel can be written as

$$D_{2^n}^{(4)} = (I_{2^{n-1}} \otimes C_1)P_{2^n}(N \otimes I_{2^{n-1}})(N \otimes I_{2^{n-2}} \oplus I_{2^{n-1}}) \dots (N \otimes I_2 \oplus I_{2^{n-4}})(N \oplus I_{2^{n-2}})P_{2^n}(I_{2^{n-1}} \otimes C_0) \quad (6)$$

where P_{2^n} is the full permutation matrix which action on the binary representation of vector indexes is $P_{2^n}(a_0, a_1, \dots, a_{n-2}, a_{n-1}) = (a_{n-1}, a_{n-2}, \dots, a_1, a_0)$ and N is the not gate. Here C_1, C_0 are 2×2 rotation matrices, which can be expressed via the Daubechies coefficients c_0, c_1, c_2, c_3 by defining

$$\begin{aligned} \tilde{C}_0 &= 2 \begin{pmatrix} c_2 & c_3 \\ c_3 & -c_2 \end{pmatrix} & \tilde{C}_1 &= \frac{1}{2} \begin{pmatrix} \frac{c_0}{c_3} & 1 \\ 1 & -\frac{c_0}{c_3} \end{pmatrix} \\ C_0 &= \frac{1}{\sqrt{\det \tilde{C}_0}} \tilde{C}_0 = \begin{pmatrix} \sin \theta_0 & \cos \theta_0 \\ \cos \theta_0 & -\sin \theta_0 \end{pmatrix} & C_1 &= \frac{1}{\sqrt{\det \tilde{C}_1}} \tilde{C}_1 = \begin{pmatrix} \sin \theta_1 & \cos \theta_1 \\ \cos \theta_1 & -\sin \theta_1 \end{pmatrix} \end{aligned} \quad (7)$$

where $\theta_0 = \frac{\pi}{3}$ and $\theta_1 = \frac{5}{12}\pi$. The operator P_{2^n} is implemented by $O(n)$ swap gates. We note a slight modification in the equation (7), comparing to [11]. The quantum circuit corresponding to the wavelet kernel (6) is shown in Fig.9. Fig.10 clarifies the notations used in Figs.8,9. The total number of elementary gates needed to implement the kernel circuit scales as $O(n^2)$, thus leading to a $O(n_q^3)$ total complexity for the QWT. For our circuit the number of elementary gates was $n_g = 1509, 2974, 5237, 8470, 12821, 18462, 25541$ for $n_q = 6, 7, 8, 9, 10, 11, 12$. It is assumed that the elementary gates act between any two qubits.

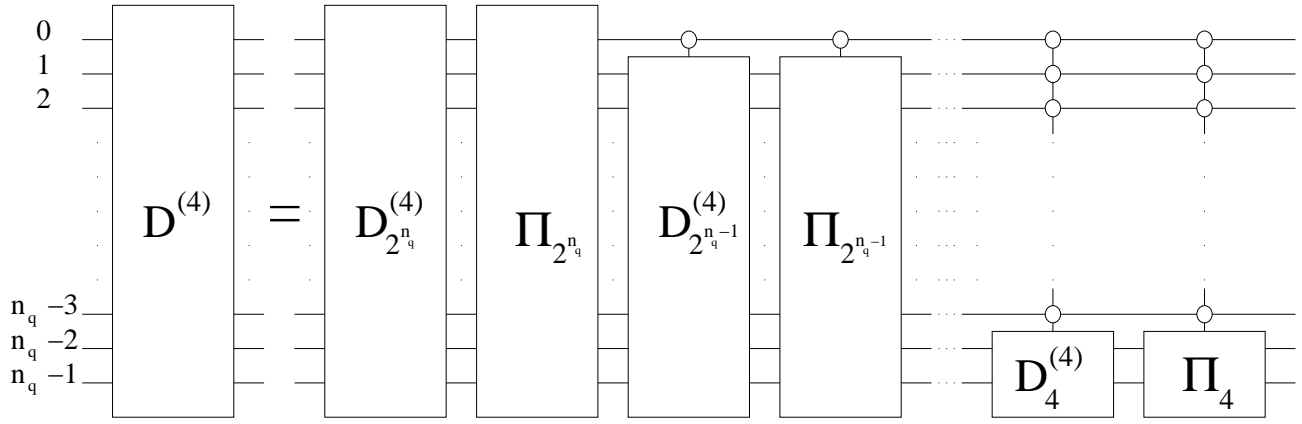
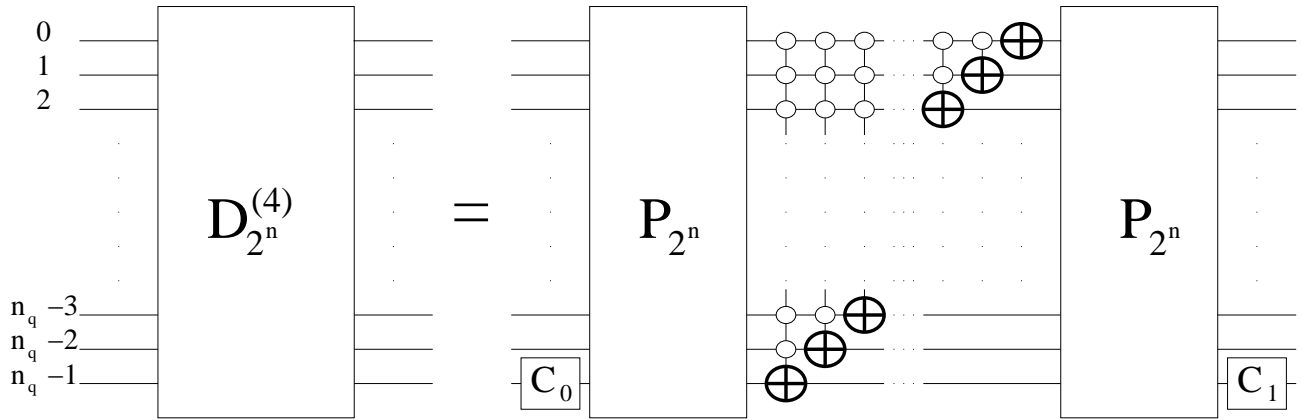
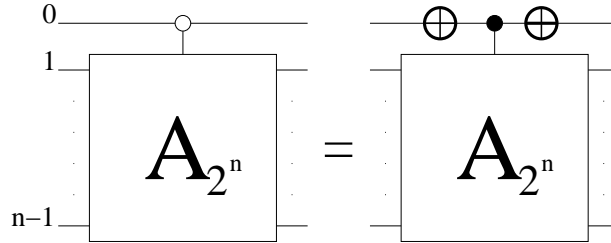


FIG. 8: Quantum circuit for the wavelet Transform (6).

FIG. 9: Quantum circuit for the wavelet kernel (6). \oplus represents the Not Operation.FIG. 10: Representation of the $(A_{2^{n-1}} \oplus I_{2^{n-1}})$ operator, \oplus is the Not Operation.

A4

Here we show the probability distribution in the computational basis for a large value of kick strength ($k = 1000$) at two different moments of time ($t = 1000$ and $t = 10000$) (Figs.11,12). We remark two main features: the distributions have pronounced peaked structure and the peaks are spread all over the computational basis. For $t = 1000$ the effects of noisy errors are weak so that exact and noisy distributions are close (top vs. middle) while the distribution for static imperfections is already strongly modified (top vs. bottom).

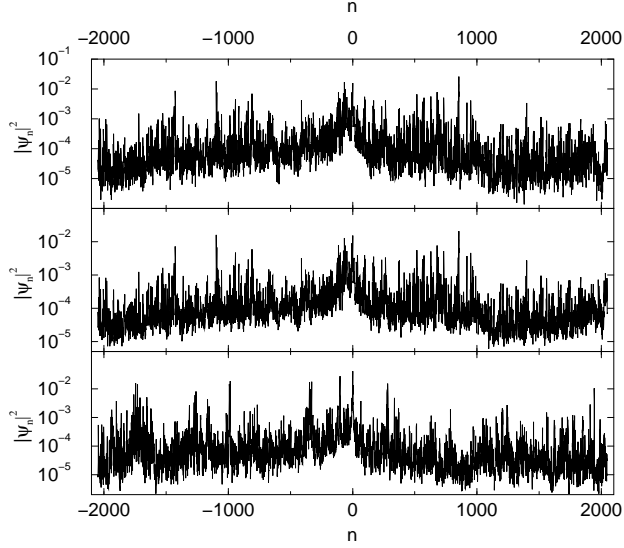


FIG. 11: Probability distribution in the computational basis for $n_q = 12$, $k = 1000$ and $t = 1000$: quantum computation with exact gates (top), with noisy gates at $\epsilon = 5 \times 10^{-4}$ (middle) and static imperfections at $\epsilon = 10^{-4}$, $\mu = 0$ (bottom).

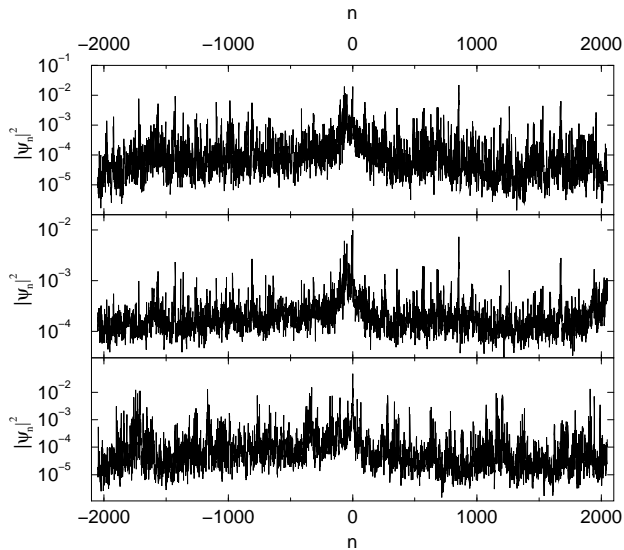


FIG. 12: Same as Fig.11 for $t = 10000$.

We have also considered another model of static imperfections. It is obtained from the model of noisy gates by repeating the same sequence of errors for each application of the evolution operator \hat{U} in (1). As in [17] each noisy gate transformation is obtained by diagonalization of nondiagonal part and then by multiplication of each eigenvalue by a random phase $\exp(i\eta)$ with $-\epsilon/2 < \eta < \epsilon/2$. This pseudo-static imperfections model is intermediate between the two cases considered in the text. The behaviour of fidelity $f(t)$ is similar to the one shown in Fig.5a (see Fig.13 (top)). For large and moderate ϵ the total number of gates N_g is not very large compared to n_g and correlations between different map iterations can be neglected. Then the gates look like quasi-random and the scaling is given by the relation (2) with $C \approx 5$. However, in the limit of small ϵ the coherent rotations become dominant and the data give the scaling $N_g \propto 1/\epsilon$ (see Fig.13). This confirms the generic scaling typical of static imperfections.

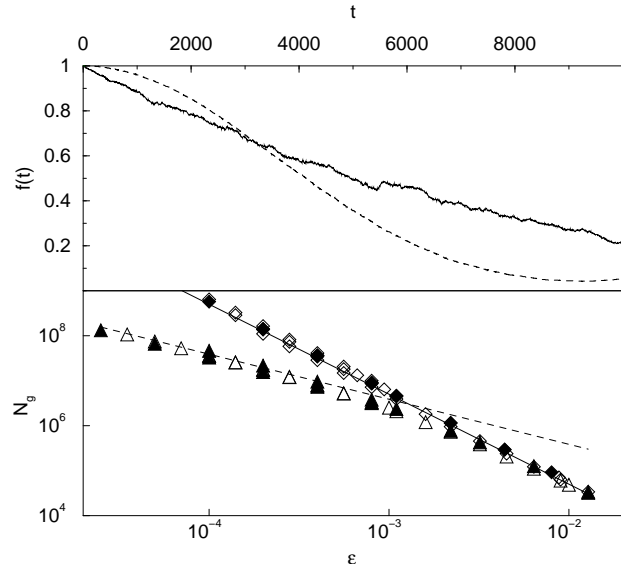


FIG. 13: Comparison between noisy gates model and pseudo-static imperfections model. Top panel shows the behaviour of the fidelity $f(t)$ for $n_g = 12$, $k = 1$, $T = 1.4$ and $\epsilon = 5 \times 10^{-4}$ (full curve for noisy gates model) and $\epsilon = 10^{-4}$ (dashed curve for pseudo-static imperfections). Bottom panel: scaling for the total number of gates N_g as a function of ϵ for noisy gates (diamonds) and pseudo-static imperfections (triangles). Open (full) symbols correspond to $k = 1$ ($k = 1000$). The full and dashed straight lines show the dependences $N_g \propto 1/\epsilon^2$ and $N_g \propto 1/\epsilon$ for noisy gates and pseudo-static imperfections respectively.

* <http://www.quantware.ups-tlse.fr>

-
- [1] I. Daubechies, *Ten Lectures on Wavelets*, CBMS-NSF Series in Applied Mathematics (SIAM, Philadelphia, 1992).
- [2] Y. Meyer, *Wavelets: Algorithms and Applications* (SIAM, Philadelphia, 1993).
- [3] M.A. Nielsen and I.L. Chuang *Quantum Computation and Quantum Information*, Cambridge Univ. Press, Cambridge (2000).
- [4] P.W. Shor, in *Proc. 35th Annual Symposium on Foundation of Computer Science*, Ed. S. Goldwasser (IEEE Computer Society, Los Alamitos, CA, 1994), p.124
- [5] R. Schack, *Phys. Rev. A* **57**, 1634 (1998).
- [6] P.H. Song and D.L. Shepelyansky, *Phys. Rev. Lett.* **86**, 2162 (2001).
- [7] G. Benenti *et al.*, *Phys. Rev. Lett.* **87**, 227901 (2001).
- [8] I. Cirac and P. Zoller, *Phys. Rev. Lett.* **74**, 4091 (1995).
- [9] C. Miguel, J.P. Paz and W.H. Zurek, *Phys. Rev. Lett.* **78**, 3971 (1997).
- [10] P. Hoyer, quant-ph/9702028 (1997).
- [11] A. Fijaney and C. Williams, *Lecture Notes in Computer Science* **1509**, 10 (Springer, 1998); quant-ph/9809004.
- [12] A. Klappenecker, in *Wavelet Applications in Signal and Image Processing VII*, Eds. M.A. Unser, A. Aldroubi, A.F. Laine, SPIE (1999) p. 703: quant-ph/9909014.
- [13] J.P. Bouchaud and A. Georges, *Phys. Rep.* **195**, 127 (1990).
- [14] A.D. Mirlin *et al.*, *Phys. Rev. E* v.54, 3221 (1996); M. L. Ndawana, V. E. Kravtsov, cond-mat/0302569 (2003).
- [15] A. Mirlin, *Phys. Rep.* **326**, 259 (2000).
- [16] A. Barenco *et al.*, *Phys. Rev. A* **52**, 345 (1995).
- [17] B. Georgeot and D.L. Shepelyansky, *Phys. Rev. Lett.* **86**, 5393 (2001).
- [18] B. Georgeot and D.L. Shepelyansky, *Phys. Rev. E* **62**, 3504 (2000); **62**, 6366 (2000).
- [19] G. Benenti *et al.*, *Eur. Phys. J. D* **20**, 293 (2002); *Eur. Phys. J. D* **22**, 285 (2003).

- [20] W.H.Zurek, Phys. Rev. Lett. **53**, 391 (1984);
V.V.Flambaum, Aust. J. Phys. **53**, 489 (2000).
[21] A.Steane, quant-ph/0207119 (2002).
[22] We thank D.Gottesman for the discussion on this point.